Inorg. Chem. **2008**, *47*, 4854−4860

Tetranuclear $[\{Ni(HL^3)\}\{W(CN)_8\}]_2$ Square: A Case of Antiferromagnetic $\{Ni^{II}W^{V}\}$ Interactions

Thengarai S. Venkatakrishnan,[†] Cédric Desplanches,[‡] Raghunathan Rajamani,[§] Philippe Guionneau,[‡] Laurent Ducasse,[||] S. Ramasesha,[*,§] and Jean-Pascal Sutter[*,†]

Laboratoire de Chimie de Coordination du CNRS, Université Paul Sabatier, 205 route de Narbonne, 31077 Toulouse, France, ICMCB, CNRS, Université Bordeaux 1, 87 Avenue du Dr A. Schweitzer, 33608 Pessac cedex, France, Solid State and Structural Chemistry Unit, Indian Institute of Science, Bangalore 560012, India, and Institut des Sciences Moléculaires, UMR 5803 du CNRS, Université Bordeaux I, 351 Cours de la Libération, 33405 Talence, France

Received January 21, 2008

A tetranuclear cyano-bridged $[\{Ni(HL^3)\}\{W(CN)_8\}]_2$ compound in a square geometry was formed by self-assembling of $\{W(CN)_8\}^{3-}$ and $\{NiL^3\}^{2+}$ (L^3 = pentadentate ligand). The structure of the compound has been established by single crystal X-ray diffraction. The coordination sphere of the Ni ions is severely distorted with the macrocyclic ligand adopting a facial coordination with only four linkages to the metal center. The N atom of the pendant aminopropyl arm of L^3 is no longer coordinated to the metal center but has undergone protonation during the assembling process. Magnetic measurements have revealed an unexpected antiferromagnetic behavior ($J = -9$ cm^{-1}), which has been explained using a microscopic many-body electronic model Hamiltonian, based on DFT results. The many-body model is used to fit both the $\chi_M T$ versus T and the M versus H plots obtained from experiments.

Introduction

Second and third row paramagnetic transition metal ions are attracting increasing interest in molecular magnetism because these ions can promote stronger exchange coupling than their 3d analogues.[1,2] For instance, cyanometallate complexes of Mo, Nb, or W have been used in association with 3d ions to prepare bimetallic magnets with rather high T_C's.[3–8] Furthermore, these building units appear well suited to obtain original low dimensional architectures such as chains[9–14] or high-nuclearity clusters.[10,15–22] For such bimetallic assemblies, Ni(II) is of special interest because this ion has been found to have significant ferromagnetic interactions with Mo(III), Mo(V), or W(V),[2,17,18,20] whereas the only example reported hitherto with Nb(IV)[10] suggests that antiferromagnetic interactions are operative. Herein we report an unusual case of antiferromagnetic {Ni−W} interaction. This has been found for a square-shaped tetranuclear $\{Ni-W\}_2$ compound formed by self-assembling of $\{W(CN)_8\}^{3-}$ and $\{NiL^3\}^{2+}$ (L^3 = pentadentate ligand).

Results and Discussion

Synthesis and Structural Features. The reaction of $(HNBu_3)_3\{W(CN)_8\}$ and $\{Ni(L^3)\}(ClO_4)_2$ (where L^3 is a pentadentate macrocyclic Schiff base ligand, Scheme 1) in H_2O produced the compound $[\{Ni(HL^3)\}\{W(CN)_8\}]_2.5H_2O$, **1**. Cubic reddish-brown single crystals have been grown by

* To whom correspondence should be addressed. E-mail: ramasesh@sscu.iisc.ernet.in (S.R.), sutter@lcc-toulouse.fr (J.-P.S.).
† Université Paul Sabatier.
‡ ICMCB, CNRS, Université Bordeaux 1.
§ Indian Institute of Science.
|| Institut des Sciences Moléculaires, UMR 5803 du CNRS, Université Bordeaux I.

(1) Beauvais, L. G.; Long, J. R. *J. Am. Chem. Soc.* **2002**, *124*, 2110–2111.
(2) Visinescu, D.; Desplanches, C.; Imaz, I.; Bahers, V.; Pradhan, R.; Villamena, F.; Guionneau, P.; Sutter, J. P. *J. Am. Chem. Soc.* **2006**, *128*, 10202–10212.
(3) Larionova, J.; Clérac, R.; Sanchiz, J.; Kahn, O.; Golhen, S.; Ouahab, L. *J. Am. Chem. Soc.* **1998**, *120*, 13088–13095.
(4) Zhong, Z. J.; Seino, H.; Mizobe, Y.; Hidai, M.; Verdaguer, M.; Ohkoshi, S.-I.; Hashimoto, K. *Inorg. Chem.* **2000**, *39*, 5095–5101.
(5) Pilkington, M.; Decurtins, S. *Chimia* **2000**, *54*, 593–601.
(6) Larionova, J.; Clérac, R.; Donnadieu, B.; Guérin, C. *Chem.—Eur. J.* **2002**, *8*, 2712–2716.
(7) Tanase, S.; Tuna, F.; Guionneau, P.; Maris, T.; Rombaut, G.; Mathonière, C.; Andruh, M.; Kahn, O.; Sutter, J.-P. *Inorg. Chem.* **2003**, *42*, 1625–1631.
(8) Milon, J.; Daniel, M.-C.; Kaiba, A.; Guionneau, P.; Brandès, P.; Sutter, J.-P. *J. Am. Chem. Soc.* **2007**, *129*, 13872–13878.

10.1021/ic800114y CCC: $40.75
Published on Web 04/09/2008

Scheme 1. Cationic moiety of $[Ni(L^3)](ClO_4)_2$

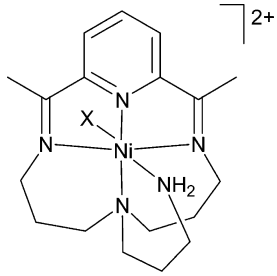

slow interdiffusion of solutions of these reagents. The investigation of the crystal structure of **1** was done by X-ray diffraction studies which revealed the formation of a tetranuclear square. A view of the molecular structure is depicted in Figure 1.

The molecular structure of **1** can be described as a square in which two $\{W(CN)_8\}$ units are linked to two Ni moieties through two bridging cyanides. The two NC bridges are cisoid. This arrangement results from a major reorganization of the coordination sphere of the Ni ions. Indeed in **1** the N atom of the pendant aminopropyl arm (labeled as N14 in structure) of L^3 is no longer coordinated to the metal center but has undergone protonation during the assembling process. Besides, the macrocylic ligand has moved from equatorial to facial-type coordination. Equatorial-to-facial coordination rearrangement is rather rare for such macrocyclic ligands,[23,24] but on/off coordination of the additional amino group by protonation has been reported.[25,26] The nickel center adopts a severely distorted coordination in which the Ni-Ligand bonds are not aligned with the directions of an octahedral geometry (Figure 1). Among the six Ni−N bond distances, four of them lie in a range 1.998(5)− 2.057(5) Å. The other

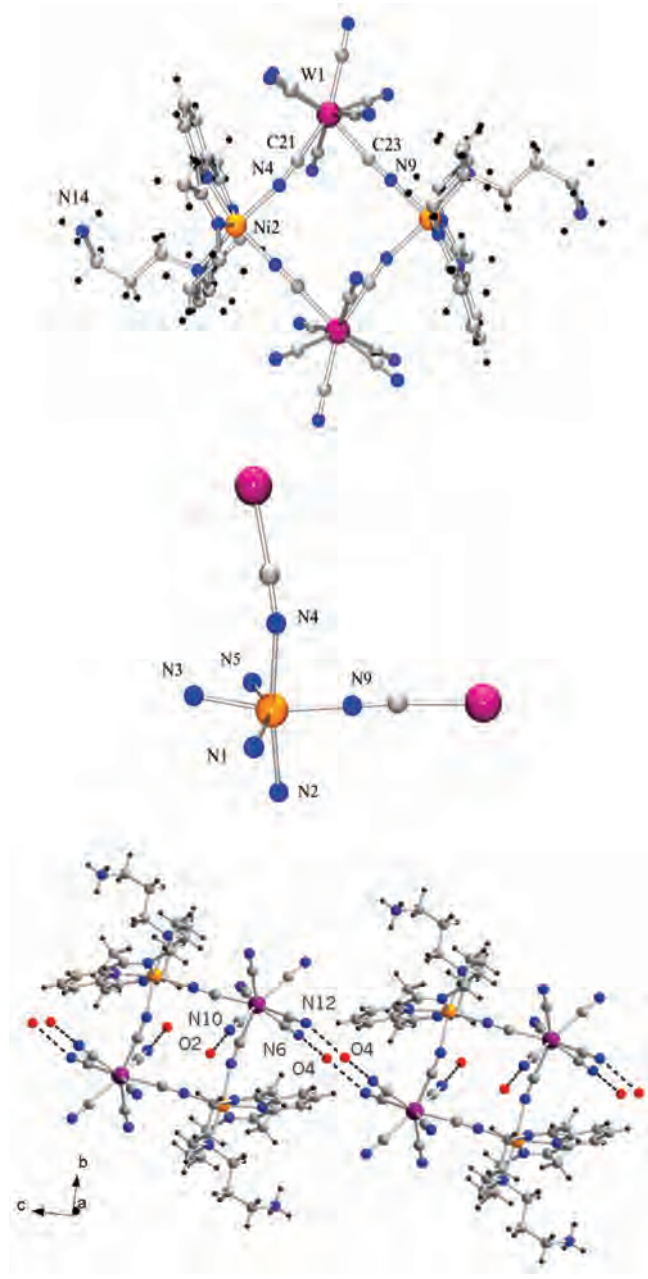

Figure 1. (top) Molecular structure for $[\{Ni(HL^3)\}\{W(CN)_8\}]_2 \cdot 5H_2O$, **1**, (middle) detail showing the distorted coordination sphere of the Ni center, and (bottom) intermolecular connections through H-bonds with H_2O (O4) taking place in the crystal. Selected bond lengths (Å) and angles (°): N1−Ni, 2.0571(8); N2−Ni, 2.1612(5); N3−Ni, 1.9978(7); N4−Ni, 2.1582(5); N5−Ni, 2.0593(9); N9−Ni, 2.0220(7); Ni···Ni, 7.309(2); W···W, 7.707(2); N6···O4, 2.919(1); N12···O4, 2.8526(6); N10···O2, 2.9559(8); Ni−N4−C21, 154.47(2); Ni−N9−C23, 178.17(2); N1−Ni−N5, 152.68(2); N3−Ni−N9, 165.55(2); N3−Ni−N5, 77.03(1); N1−Ni−N3, 77.38(1); N1−Ni−N9, 102.13(1); N2−Ni−N4, 172.37(1); N4−Ni−N9, 84.00(1); N2−Ni−N3, 105.78(1).

two Ni−N distances are significantly larger [2.158(5) and 2.161(5) Å]. The two Ni ← N≡C bond distances are different with 2.158(5) (Ni−N4) and 2.022(5) Å (Ni−N9). The central nitrogen atom bound to the propyl ammonium group makes a long bond to the nickel center [Ni−N2, 2.161(5) Å]. Analysis of the geometry around tungsten with the SHAPE[27] program shows that the cyanometallate adopts dodecahedral geometry,[28] the results are tabulated in the Supporting Information. The W−C−N angles are almost linear and are

(9) Li, D.; Gao, S.; Zheng, L.; Tang, W. *Dalton Trans.* **2002**, 2805–2806.
(10) Pradhan, R.; Desplanches, C.; Guionneau, P.; Sutter, J.-P. *Inorg. Chem.* **2003**, *42*, 6607–6609.
(11) Ikeda, S.; Hozumi, T.; Hashimoto, K.; Ohkoshi, S.-I. *Dalton Trans.* **2005**, 2120–2123.
(12) Przychodzen, P.; Lewinski, K.; Pelka, R.; Balanda, M.; Tomala, K.; Sieklucka, B. *Dalton Trans.* **2006**, 625–628.
(13) Prins, F.; Pasca, E.; de Jongh, L. J.; Kooijman, H.; Spek, A. L.; Tanase, S. *Angew. Chem., Int. Ed.* **2007**, *46*, 6081–6084.
(14) Withers, J. R.; Li, D.; Triplet, J.; Ruschman, C.; Parkin, S.; Wang, G.; Yee, G. T.; Holmes, S. M. *Polyhedron* **2007**, *26*, 2353–2366.
(15) Larionova, J.; Gross, M.; Pilkington, M.; Andres, H.; Stoeckli-Evans, H.; Güdel, H. U.; Decurtins, S. *Angew. Chem. Int. Ed.* **2000**, *39*, 1605–1609.
(16) Zhong, Z. J.; Seino, H.; Mizobe, Y.; Hidai, M.; Fujishima, A.; Ohkoshi, S.-I.; Hashimoto, K. *J. Am. Chem. Soc.* **2000**, *122*, 2952–2953.
(17) Bonadio, F.; Gross, M.; Stoeckli-Evans, H.; Decurtins, S. *Inorg. Chem.* **2002**, *41*, 5891–5896.
(18) Shores, M. P.; Sokol, J. J.; Long, J. R. *J. Am. Chem. Soc.* **2002**, *124*, 2279–2292.
(19) Song, Y.; Zhang, P.; Ren, X.-M.; Shen, X.-F.; Li, Y.-Z.; You, X.-Z. *J. Am. Chem. Soc.* **2005**, *127*, 3708–3709.
(20) Lim, J. H.; Yoon, J. H.; Kim, H. C.; Hong, C. S. *Angew. Chem., Int. Ed.* **2006**, *45*, 7424–7426.
(21) Zhao, H.; Shatruk, M.; Prosvirin, A. V.; Dunbar, K. R. *Chem.−Eur. J.* **2007**, *13*, 6573–6589.
(22) Venkatakrishnan, T. S.; Rajamani, R.; Ramasesha, S.; Sutter, J.-P. *Inorg. Chem.* **2007**, *46*, 9569–9574.
(23) Thöm, V. J.; Fox, C. C.; Boeyens, J. C. A.; Hancock, R. D. *J. Am. Chem. Soc.* **1984**, *106*, 5947–5955.
(24) Guilard, R.; Siri, O.; Tabard, A.; Broeker, G.; Richard, P.; Nurco, D. J.; Smith, K. M. *J. Chem. Soc., Dalton Trans.* **1997**, 3459–3463.
(25) Siegfried, L.; Kaden, T. A. *Dalton Trans.* **2005**, 3079–3082.
(26) Taktak, S.; Ye, W.; Herrera, A. M.; Rybak-Akimova, E. V. *Inorg. Chem.* **2007**, *46*, 2929–2942.

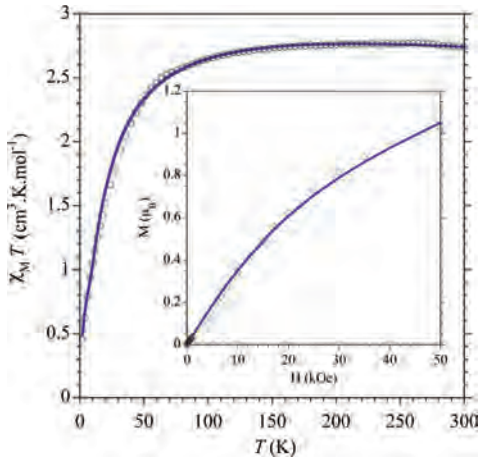

Figure 2. Experimental (open circle) and calculated (solid line) temperature dependence of $\chi_M T$ for **1**, (inset) experimental and calculated field dependence of the magnetization at 2 K. Best fit parameters: $J = -9.0$ cm^{-1}, $J' = -0.75$ cm^{-1}, $D = -0.32$ cm^{-1}, and $g = 2.16$ (see text).

in the range 175.5(5)−179.0(7)°. The two cyanide ligands involved in bridging to nickel make angles of 176.1° (W−C21−N4) and 178.2° (W1−C23−N9) with W while the angles with Ni are 154.5° (Ni−N4−C21) and 178.2° (Ni−N9−C23). Six terminal cyanide ligands of **1** are involved in hydrogen bonding with H_2O molecules, four of which are acting as bridges between tetranuclear units. The overall supramolecular organization consists in 1D-arrays of H_2O linked squares (Figure 1).

Magnetic Properties

The magnetic behavior of **1** was investigated in the temperature domain 2−300 K on a polycrystalline sample in an applied field of $H = 1000$ Oe. The temperature dependence of the product of molar magnetic susceptibility, χ_M, and temperature is shown in Figure 2. The $\chi_M T$ product at 300 K is 2.74 cm^3 K mol^{-1}, in agreement with the paramagnetic contribution of two $S = 1$ {NiL^3} and two $S = 1/2$ {W(CN)$_8$}$^{3-}$ spin moieties (2.75 cm^3 K mol^{-1}, $g = 2.0$). This value remains unchanged down to 100 K, and then, it begins to drop steeply reaching 0.46 cm^3 K mol^{-1} at 2 K. The field dependence of the magnetization recorded at 2 K (inset Figure 2) is characterized by a slow increase to 1.05 μ_B for 5 T, the highest field investigated. Both $\chi_M T$ versus T and M versus H reveal the occurrence of antiferromagnetic interactions within **1**, a behavior in strong contrast to the previously reported example of Ni−W interactions (vide supra).

The structural information for **1** have revealed significantly different geometric features for the two Ni ← NC linkages; moreover, the {W(CN)$_8$} unit has its bridging CN located on each of the two coordination sites occurring for a dodecahedron geometry.[2] As a consequence, two distinct pathways might be operative for **1**. The three possible interaction schemes for such a tetranuclear spin system are given in

Scheme 2. Possible interaction schemes for **1** and corresponding spin ground states (S_{gs}). Negative J refers to antiferromagnetic interaction

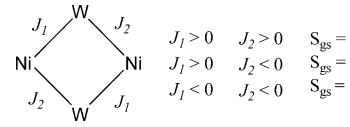

Scheme 2. These are characterized by specific ground states. Obviously, the magnetic behavior of **1** permits to exclude the first case with $S = 3$. To discriminate between the two other cases, the experimental magnetic data have been analyzed by a theoretical model.

In a first attempt to fit the magnetic behavior of **1**, we have considered the possibility of two exchange pathways, one ferromagnetic and one antiferromagnetic. However, the analytical parameters did not converge to values with physical meaning. The experimental data have then been analyzed by considering a single antiferromagnetic interaction J, where J is an average of J_1 and J_2. The spin Hamiltonian employed for the fit is

$$\hat{H}_1 = -J\sum_{i=1}^{4} \hat{S}_i \cdot \hat{S}_{i+1} \quad (1)$$

Cyclic boundary condition $\hat{S}_5 = \hat{S}_1$ is implied here and below. Together with the anisotropy term (D) and the intermolecular interaction (J'), the perturbing Hamiltonian is given by

$$\hat{H}_2 = -zJ'\langle S_z\rangle\sum_{i=1}^{4} \hat{S}_{i,z} + g\mu_B H\sum_{i=1}^{4} \hat{S}_{i,z} + D\hat{S}^2_{z,\mathrm{tot}} \quad (2)$$

where, we have used the same g values for Ni(II) and W(V) ions. The total Hamiltonian used for the fit is

$$\hat{H} = \hat{H}_1 + \hat{H}_2 \quad (3)$$

If, $E_0(S,M_S)$ are the eigenvalues of the unperturbed Hamiltonian, $\hat{H}_1$, then the eigenstates of $\hat{H}_1$, in the mean-field approximation is given by

$$E(S, M_s) = E_0(S, M_s) - zJ'\langle S_z\rangle M_s + g\mu_B H M_s + DM_s^2 \quad (4)$$

where

$$\langle S_z\rangle = \frac{\sum_S \sum_M M_s e^{-(E_0(S,M_s)+DM_s^2)/k_B T}}{\sum_S \sum_M e^{-(E_0(S,M_s)+DM_s^2)/k_B T}} \quad (5)$$

The molar magnetic susceptibility is given by

$$\chi_M = \frac{Ng^2\mu_B^2\langle M_s^2(J,T)\rangle}{k_B T - zJ'\langle M_s^2(J,T)\rangle} \quad (6)$$

and the magnetization ⟨M⟩ is given by

$$\langle M\rangle = Ng\mu_B\langle \hat{S}_z\rangle \quad (7)$$

For small intermolecular interactions and D, $\langle M_s^2(J.T)\rangle$ in eq 6 is obtained as

(27) Llunell, M.; Casanova, D.; Cirera, J.; Bofill, J. M.; Alemany, P.; Alvarez, S.; Pinsky, M.; Avnir, D. *SHAPE*, 1.1b; University of Barcelona: Barcelona, 2005.
(28) Casanova, D.; Llunell, M.; Alemany, P.; Alvarez, S. *Chem.—Eur. J.* **2005**, *11*, 1479–1494.

$$\langle M_s^2(J,T)\rangle = \frac{\sum_S \sum_M M_s^2 e^{-(E_0(S,M_s)+DM_s^2)/k_BT}}{\sum_S \sum_M e^{-(E_0(S,M_s)+DM_s^2)/k_BT}} \quad (8)$$

The best fit to the experimental data (Figure 2) has been obtained for $J = -9.0$ cm^{-1}, $zJ' = -3.0$ cm^{-1} (i.e., $J' = -0.75$ cm^{-1} per neighbor), $g = 2.16$, and $D = -0.32$ cm^{-1}. Though, the spin model shows that the superexchange interaction in this system is antiferromagnetic, it does not provide the reason for the anomaly.

Theoretical Studies. In a previous Density Functional Theory (DFT) study, we have shown that the exchange interaction for a d^1 $\{M(CN)_8\}$ unit (M = Mo^V, Nb^{IV}, W^V) with Ni^{II} in an octahedral surrounding is anticipated to be ferromagnetic because of the orthogonality of the magnetic orbitals emanating from the metal centers,[2] in accordance with the Goodenough−Kanamori (G-K) rules. Therefore, the magnetic interaction found for **1** is rather intriguing. Several hypotheses can be put forward to account for the antiferromagnetic superexchange, for instance the severe deviation of the nickel units from an octahedral geometry or the strongly bent Ni−N≡C angle occurring in **1**. With the aim of gaining some insights on the origin of the observed behavior, DFT modeling of this system was undertaken.

The DFT calculations have been carried out on two dinuclear [{(CN)Ni(HL)}{W(CN)$_8$}] fragments of **1**, each corresponding to a different W−CN−Ni linkage geometry (i.e., Ni−N9−C23−W and Ni−N4−C21−W), for the high spin-state $S = 3/2$. The magnetic orbitals, defined as the natural orbitals for the high spin state, have been computed and are reported in Figure 3. It is known from Kahn's model that the sign of the magnetic interaction depends on the symmetry of the so-called magnetic orbitals. In a dinuclear fragment, these orbitals are defined as the singly occupied orbitals (SOMOs) of each metal and its surrounding diamagnetic organic ligands. For $\{W(CN)_8\}^{3-}$ in a dodecahedron environment, the SOMO is anticipated to result from a mixing of the nondegenerate d_{xy} metal centered orbital with the π-orbitals of the cyanide ligands, whereas on the Ni side, the SOMOs should result from the mixing of the σ-system of the ligands (i.e., the HL^3 macrocycle and the N-bound cyanides) with the metal centered $d_{x^2-y^2}$ and d_{z^2} orbitals. Therefore, no overlap is expected between the W and Ni centered SOMOs, and the exchange interaction should be ferromagnetic.[2] However, this will only remain true as long as the geometry of the Ni unit is octahedral. This is no longer the case for **1** where a strong deformation of the coordination sphere for Ni is found (Figure 1). As a result, for both the linear (Ni−N−C, 178.2°) and bent (Ni−N−C, 154.5°) geometries, it can be observed that most of the orbitals have a contribution on the two Ni and W metals. This indicates that strict orthogonality does not apply between the magnetic orbitals located on the metal centers. According to the so-called Kahn model,[29] overlap of magnetic orbitals tends to favor the antiferromagnetic state as a ground state. Thus for **1** antiferromagnetic Ni−W interactions can be expected through the two exchange pathways, and this result might support the third case of Scheme 2. While the DFT study seems to indicate the possibility of antiferromagnetic interactions, it remains inconclusive. Indeed, attempts to calculate the low-spin state have failed because of convergence problems, and thus, it has not been possible to evaluate numerically the J coupling parameter.

To pursue the modeling of the magnetic property further, we have used a phenomenological microscopic model that is quantitative and goes beyond Kahn's model. The Kahn model for magnetic interaction between the magnetic orbitals is an attempt to quantify semiempirically the G-K rules. In this model, the effective exchange interaction depends upon the direct exchange integral involving magnetic orbitals, the transfer integral between magnetic orbitals, the site energies of the magnetic orbitals, and other electron repulsion integrals, as well as the overlap integral between the magnetic orbitals. In this approach, a nonzero overlap integral, P, favors antiferromagnetic interaction in the first order, while in the second order (the P^2 term) it could contribute to either ferromagnetic or antiferromagnetic superexchange depending upon the one and two electron parameters. The direct exchange integral always favors a ferromagnetic superexchange pathway. DFT calculations carried out on a dinuclear fragment of W and Ni in **1** yields the three singly occupied molecular orbitals (MOs) shown in Figure

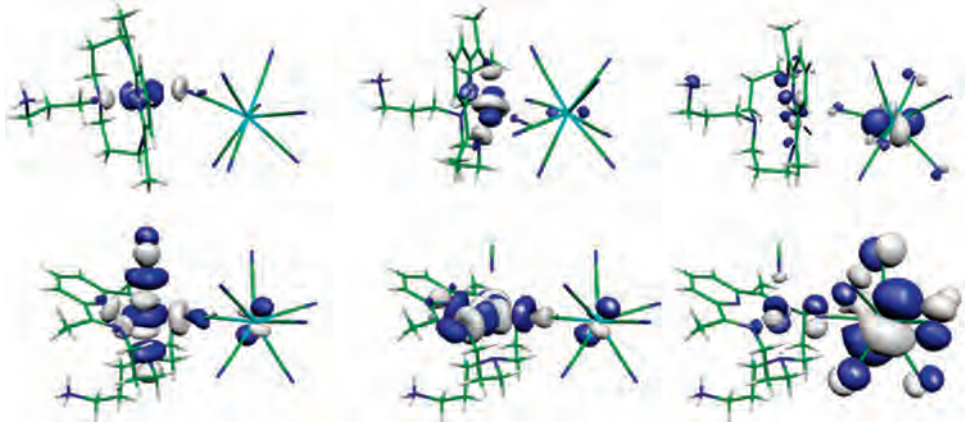

Figure 3. Singly Occupied Molecular Orbitals (SOMOs) deduced from DFT calculations of the $\{(CN)_2Ni(HL^3)(NC)W(CN)_7\}$ fragments of **1** (top, Ni−N4−C21−W; bottom, Ni−N9−C23−W (the Ni−ligand bonds are not depicted for clarity).

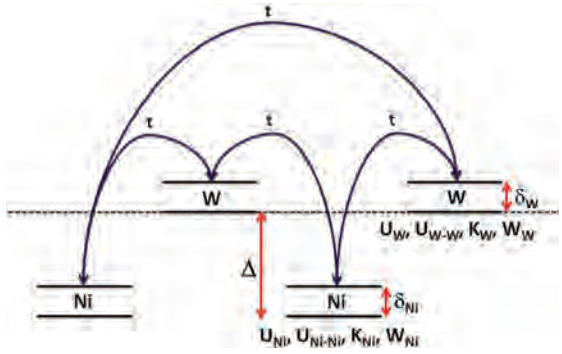

Figure 4. Schematic of the microscopic model for superexchange in $\{NiW\}_2$ cluster. For simplicity, we have taken all transfer integrals, t, to be the same. Other parameters are explained in the text.

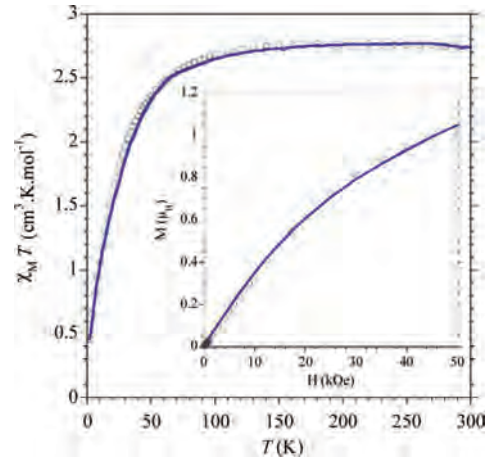

Figure 5. Experimental (open circle) and calculated (solid line, from the electronic model) temperature dependence of $\chi_M T$ for **1**, (inset) experimental and calculated (from the electronic model) field dependence of the magnetization at 2 K. The best fit parameters are $J_{eff} = -10.66$ cm^{-1}, $J' = -0.87$ cm^{-1}, $D = -0.39$ cm^{-1}, and $g = 2.16$ obtained with (in eV) $t = 0.1$, $\Delta = 0.5$; $\delta_{Ni} = 0.4$, $\delta_W = 0.1$, $U_{Ni} = 7.0$, $U_W = 8.0$, $U_{Ni-Ni} = 4.5$, $U_{W-W} = 5.7$, $K_{Ni} = 0.7$, $K_W = 0.3$, $W_{Ni} = 1.0$, $W_W = 1.0$.

3. Furthermore, the energies of the two singly occupied MOs on Ni are split by about 0.4 eV (3150 cm^{-1}). These results allow us to construct a phenomenological microscopic model involving the active orbitals in the $\{NiW\}_2$ square complex **1**, along the lines of an earlier theoretical study reported for binuclear transition metal clusters.[30] In that model, we showed that the final outcome of a superexchange process depends upon the occupancies of the orbitals involved in superexchange, the magnitude of transfer parameters, the magnitude of the splitting of the energy levels involved in superexchange, and finally on the intra-atomic electron repulsion integrals.

The orbitals considered in our phenomenological model are the e_g orbitals on Ni and two low-lying 5d orbitals of W. It is known from the DFT calculations that the e_g levels on Ni(II) ions for **1** are split with an energy gap, δ_{Ni} of 0.4 eV. The two orbitals on W(V) are also similarly split by an amount δ_w. The K_{Ni} and K_W are the direct exchange integrals on Ni and W, respectively. U_{Ni} and U_W are the intraorbital electron repulsion parameters (Hübbard parameters) for Ni and W, and similarly, the on-site interorbital repulsion parameters are U_{Ni-Ni} and U_{W-W}. The intersite electron−electron interactions are parametrized using the Ohno scheme.[31,32] The electron transfer integrals mix the various electronic configurations. A schematic of the model is shown in the Figure 4.

It is interesting to qualitatively understand the role played by each of the model parameters. A large δ_{Ni} favors a diamagnetic Ni ion. Of course, this is possible if U_{Ni} is comparable to U_{Ni-Ni} and K_{Ni} is small. If U_{Ni} is large compared to U_{Ni-Ni}, then both the e_g orbitals will be singly occupied. If in addition, K_{Ni} is also large, then the spin of the electrons in the singly occupied orbitals prefer to align in parallel. A similar scenario can be envisaged for the W site, if an electron hops from the Ni site to the singly occupied W site. The transfer term in the model indeed creates such virtual intermediate states.

The superexchange process involving electron hop from Ni to W would favor ferromagnetism, if the high-spin state of W(IV) has a lower energy than the low-spin state. On the other hand, in this minimal model, the electron hop from W to spin-1 Ni(II) ion is always antiferromagnetic due to Pauli's exclusion principle. In most common cases, this hopping process results in a high-energy intermediate state and hence is not favored. However, if the splitting of the e_g orbitals on Ni is large and the center of gravity of the e_g states of Ni is below that of the two orbitals on the W site (Δ in Figure 4), then hopping from W site to Ni site is favored and the resultant superexchange interaction would be antiferromagnetic. This process would also lead to a slight decrease in the spin on Ni(II) ion from the usual value of one. Indeed, our calculations, which fit the experimental data, have a Ni(II) spin of 0.9941.

In the analysis of our magnetic data, we employ the electronic model introduced in our earlier work and solve for all the eigenstates of the model in different total spin sectors ($S = 3, 2, 1, 0$). From these eigenstates, we obtain the theoretical χ_MT versus T and the M versus H plots for the $\{NiW\}_2$ system. The eigenvalues $E_0(S,M_s)$ in eqs 4, 5, and 8 are replaced by the eigenvalues of our electronic Hamiltonian. We also introduce the single ion anisotropy and intermolecular interactions as were employed in the pure spin Hamiltonian. We show the fits of the experimental magnetic data with our model in Figure 5. Our model thus accounts for the observed antiferromagnetic exchange interactions in these systems and provides a microscopic understanding of the origin of the unusual antiferromagnetic interaction observed in the Ni−W system. From the energy gap between the ferromagnetic high-spin ($S = 3$) and the antiferromagnetic low-spin ($S = 1$) states for the best fit parameters, we can obtain an effective superexchange constant J_{eff} (the exchange parameter in equation 1), which is found to be −10.66 cm^{-1} (−15.34 K). J_{eff} from the electronic Hamiltonian is slightly different from that of the spin-only Hamiltonian ($J = -9.0$ cm^{-1}); the former includes many more states in each spin sector because electron hop allows

(29) Kahn, O. *Molecular Magnetism*; VCH: Weinheim, 1993.
(30) Raghunathan, R.; Sutter, J.-P.; Ducasse, L.; Desplanches, C.; Ramasesha, S. *Phys. Rev. B* **2006**, *73*, 104438–104448.
(31) Ohno, K. *Theor. Chim. Acta* **1964**, 2219.
(32) Klopmann, G. *J. Am. Chem. Soc.* **1964**, *86*, 4550–4557.

transition metal ions with different oxidation states in the many-body basis.

Concluding Remarks

One of the most important characteristics of the cyanide-bridge compounds is that their magnetic behavior can be predicted in sign and relative strength; therefore, it is possible to tune the material properties simply by varying the metal ions. It is the distribution of the unpaired electrons in the d orbitals of each metal site that dictates the overall exchange interaction outcome. This rather simple model is very reliable, but a severe geometrical deformation such as large deviation from 180° of the M−CN−M′ angle may lead to a discrepancy between the anticipated and observed behavior.[33] With compound **1** we show that a strong deformation of the coordination sphere of M′ (i.e., Ni for **1**) can have a related effect. Incorporating this feature in a many-body electronic model Hamiltonian provides an excellent fit for the experimental magnetic studies. The peculiar coordination sphere of the Ni ion and the concomitant lifting of the degeneracy of the d levels leads to a mixing of the metal centered singly occupied orbital which result in an overall antiferromagnetic {Ni−W} interaction.

Experimental Section

The compounds (HNBu)$_3${W(CN)$_8$},[34] {Ni(L^3)}(ClO$_4$)$_2$[35] were prepared by reported procedures. Infrared spectra were recorded as KBr pellets in the range 4000−400 cm^{-1} by using a Perkin-Elmer spectrum GX 2000 FTIR spectrometer. Elemental analyses were performed using Perkin-Elmer 2400 series II instrument. Magnetic measurements down to 2 K were carried out with a Quantum Design MPMS-5S SQUID susceptometer on polycrystalline samples. Magnetic data were corrected for core diamagnetic contributions estimated from Pascal tables and for the sample holder (gelatin capsule) contribution.

Synthesis of [{Ni(HL^3)}$_2${W^V(CN)$_8$}$_2$]·5H$_2$O, 1. {Ni(L^3)}(ClO$_4$)$_2$ (35 mg, 0.06 mmol) was dissolved in water (15 mL) by warming the solution to 55 °C. To this solution was added (HNBu)$_3$-{W(CN)$_8$} (30 mg, 0.03 mmol) in ethanol (10 mL) as a layer, and the mixture left for crystallization in dark at ambient temperature. Well formed dark red crystals suitable for X-ray diffraction were formed after 5 days along the sides of the tube. The crystals were isolated, washed with water, ethanol, and ether, and dried in air to obtain the pure compound. Yield: 8 mg (8%, based on Ni); IR ν_{CN} (KBr, cm^{-1}): 2104(s), 2120(sh), 2135(m), 2153(m), 2197(m). Elemental analysis for $C_{52}H_{69}N_{26}O_{4.5}Ni_2W_2$ calcd: %C 38.66, H 4.31, N 22.54; found: %C 38.63, H 4.75, N 22.20.

DFT Calculations. The hybrid B3LYP functional has been used as implemented in Gaussian98. The basis used in all calculation is the D95 Dunning/Huzinaga valence double-ζ for first row elementsand the small-core Hay−Wadt pseudopotential for transition metals (indicated in the Gaussian code as LANL2DZ). The natural orbitals represented have been computed with Gaussian98.

Table 1. Crystallographic Data for **1** at Room Temperature

empirical formula	$C_{26}H_{30}N_{13}NiO_{2.50}W$
formula weight	807.19
crystal system	monoclinic
space group	$P2_1/n$
unit cell dimensions	a = 11.476(5) Å b = 20.003(5) Å c = 14.785(5) Å β = 92.88(1)°
volume	3390(2) Å^3
density	1.582
absorption coefficient	3.991 mm^{-1}
F(000)	1596
theta range for data collection	4.10 to 26.37°
reflections collected	22011
independent reflections	6869 [R(int) = 0.0389]
data/restraints/parameters	6869/0/386
goodness-of-fit on F^2	0.995
final R indices [I > 2sigma(I)]	R_{obs} = 0.0363, wR2 = 0.0934
R indices (all data)	R_{all} = 0.0537, wR2 = 0.1038
largest diff. peak and hole	1.370 and −0.680 e Å^{-3}

Many-Body Model Studies. The Hamiltonian for the microscopic electronic model is given by

$$\hat{H} = 2(\Delta - \delta_{Ni})\hat{n}_{Ni} + 2\Delta\hat{n}_{Ni} + 2\delta_W\hat{n}_W + \sum_{\langle i,j\rangle} t(\hat{E}_{ij} + \hat{E}_{ji}) + \sum_i \frac{U_i}{2}\hat{n}_i(\hat{n}_i - 1) + \sum_{i,i'} \{U_{ii'}\hat{n}_i\hat{n}_{i'} + \frac{W_{ii'}}{2}[(E_{ii'} + E_{i'i})(\hat{n}_i + \hat{n}_{i'}) + (\hat{n}_i + \hat{n}_{i'})(E_{ii'} + E_{i'i}) - 2(E_{ii'} + E_{i'i})] + \frac{K_{ii'}}{2}(E_{ii'}E_{ii'} + E_{i'i}E_{i'i} + E_{ii'}E_{i'i} + E_{i'i}E_{ii'} - \hat{n}_i - \hat{n}_{i'})\} + \sum_{\langle i,j\rangle} \frac{V_{ij}}{2}\hat{n}_i\hat{n}_j$$

with

$$\hat{n}_i = \sum_\sigma a^+_{i\sigma}a_{i\sigma}; \quad \hat{E}_{ij} = \sum_\sigma a^+_{i\sigma}a_{j\sigma}$$

where Δ is the energy difference between the lower orbital on the Ni site and that on the W site, δ_{Ni} and δ_W are the splitting between the d orbitals on Ni and W sites, respectively, t is the transfer integral, U_i is the intraorbital electron−electron repulsion (Hübbard parameter), $U_{ii'}$ is the interorbital electron−electron repulsion parameter for electrons in sites i and i', $K_{ii'}$ is the direct exchange parameter, and $W_{ii'}$ is the electronic repulsion parameter between an electron residing in an orbital i and the other residing in the overlap charge cloud of the orbitals i and i'. V_{ij} is the intersite electron−electron repulsion parameter between the sites i and j. The model is solved in each spin sector for a given set of parameters by employing the valence bond method.[36] The number of S = 0, 1, 2, and 3 states are 1176, 1512, 420, and 28, respectively. The $\chi_M T$ versus T and M versus H plots in Figure 5 are obtained using eqs 5−8.

X-Ray Diffraction. Large samples being twinned, a small needle shape red dark single crystal of approximate dimensions 0.10 × 0.02 × 0.02 mm^3 was selected on a polarized microscope and mounted on a Bruker-Nonius κ-CCD diffractometer, Mo Kα radiation (0.71073 Å), mixed ϕ and ω scans, 1.6° per rotation frame, 200 s per frame, distance crystal-detector of 30.0 mm. The structural determination was carried out by direct methods, and the refinement of atomic parameters based on full-matrix least-squares on F^2 were performed using the SHELX-97 programs[37] within the WINGX package.[38] Results are summarized in Table 1.

(33) Marvaud, V.; Herrera, J. M.; Barilero, T.; Tuyeras, F.; Garde, R.; Scuiller, A.; Decroix, C.; Cantuel, M.; Desplanches, C. *Monatsh. Chem.* **2003**, *134*, 149–163.
(34) Dennis, C. R.; van Wyk, A. J.; Basson, S. S.; Leipoldt, J. G. *Transition Met. Chem.* **1992**, *17*, 471–473.
(35) Rybak-Akimova, E. V.; Nazarenko, A. Y.; Silchenko, S. S. *Inorg. Chem.* **1999**, *38*, 2974–2980.
(36) Ramasesha, S.; Soos, Z. G. In *Valence Bond Theory*; Cooper, D. L., Ed.; Elsevier Science: Amsterdam, 2002; p 635.

Acknowledgment. This work was supported by the Centre Franco-Indien pour la Promotion de la Recherche Avancée/ Indo-French Centre for the Promotion of Advanced Research (CEFIPRA/IFCPAR Project 3108−3). The computing resources were generously made available by the CINES and by the "Pôle de Modelisation" of the Institute of Molecular Sciences in Bordeaux (SGi Linux cluster).

(37) Sheldrick, G. M. *Programs for Crystal Structure Analysis*, (Release 97−2); University of Göttingen: Göttingen, Germany, 1998.
(38) Farrugia, L. J. *J. Appl. Crystallogr.* **1999**, *32*, 837.

Supporting Information Available: X-ray crystallographic file in CIF format for **1**, results of SHAPE analysis, and selected bond distances and angles (PDF). This material is available free of charge via the Internet at http://pubs.acs.org.

IC800114Y